nature geoscience

Article https://doi.org/10.1038/s41561-023-01204-4

Highly variable friction and slip observed at Antarctic ice stream bed

In the format provided by the authors and unedited

Supplementary Information for:

Highly variable friction and slip observed at Antarctic ice stream bed

T.S. Hudson[1]*, SK Kufner[2], A.M. Brisbourne[2], JM Kendall[1], A.M. Smith[2], R. Arthern[2], R.B. Alley[3], T. Murray[4]
Correspondence to: thomas.hudson@earth.ox.ac.uk

The supplementary information includes:

Supplementary Text
Figs. S1 to S6
Table S1

Further Notes:
Equation numbering continues from the main text and methods.

Supplementary Text

1. Sensitivity analysis of our simple rate-and-state friction model

A number of observations are derived from the icequake observations and input into the rate-and-state friction model. A number of these observations can vary by an order of magnitude. Extended Data Fig. 5 shows the results of a sensitivity analysis to various observational and rate-and-state model derived parameters. Each parameter is varied by a realistic factor (see Table S1 for the exact values used), in isolation.

Extended Data Fig. 5 shows that the rate-and-state model is approximately insensitive to perturbations in f_c and v/v_0. Furthermore, although the slip is approximately linearly proportional to variations in $t_{inter-event}$, the fault-area, A, and G_{bed}, the frictional shear-stress, τ_{bed} is invariant to these parameters. Larger, but still less than or approximately linear relationships are found for earthquake stress-drop, $\Delta\tau$, seismic moment, M_0, and effective normal stress, $\bar{\sigma}$.

Parameter	Mean value	Lower perturbation (and factor)	Upper perturbation (and factor)
$\boldsymbol{\tau_{bed,ref}}$	$358\ kPa$	n/a	n/a
$\boldsymbol{v_{slip,ref}}$	$0.8\ m\ day^{-1}$	n/a	n/a
$\boldsymbol{v/v_0}$	38,900	3,890 (x 0.1)	389,000 (x 10)
$\boldsymbol{\bar{\sigma}}$	$646\ KPa$	$64.6\ KPa$ (× 0.1)	$6.46\ MPa$ (× 10)
$\boldsymbol{t_{inter-event}}$	$603\ s$	$60.3\ s$ (× 0.1)	$6030\ s$ (× 10)
$\boldsymbol{M_0}$	$2.47 \times 10^7\ Nm$	$2.47 \times 10^6\ Nm$ (× 0.1)	$2.47 \times 10^8\ Nm$ (× 10)
$\boldsymbol{G_{bed}}$	$0.107\ GPa$	$0.0107\ GPa$ (× 0.1)	$1.07\ GPa$ (× 10)
A	$721\ m^2$	$72.1\ m^2$ (× 0.1)	$7210\ m^2$ (× 10)
$\boldsymbol{f_c}$	$68\ Hz$	$18\ Hz$ (−50)	$118\ Hz$ (+50)
$\boldsymbol{\Delta\tau}$	$72.0\ KPa$	$7.20\ KPa$ (× 0.1)	$720\ KPa$ (× 10)
$\boldsymbol{(a-b)}$	-0.01	−0.001 (× 0.1)	−0.01 (× 1)

Table S1. Average and perturbation values used in rate-and-state friction model sensitivity analysis.

One can also consider what the dominant observational constraints of our simplified rate-and-state formulation are. The key equation that our icequake observations constrain in our simplified assumption is Equation 13, specifically the terms $\Delta\tau$ and $\frac{v}{v_0}$. $\Delta\tau$ is given by Equation 4, being dependent on the seismic moment, M_0, and the fault radius. The seismic moment for our data varies by ~1 order of magnitude[29], and fault radius with our approximations can vary only with the free parameter f_c (see Equation 3). Similarly, $\frac{v}{v_0}$ is also dependent on f_c, but also crucially $t_{inter-event}$ (see Equation 12). Therefore, the thee dominant parameters obtained from the seismic data are: M_0, f_c, and $t_{inter-event}$. A factor 10 variation in M_0 gives a factor 10 variation in $\Delta\tau$. A factor 5 variation in f_c gives a factor 125 variation in $\Delta\tau$. Therefore, combined, $\Delta\tau$ varies by a factor 1250. If $t_{inter-event}$ also varies by a factor 10, then $\frac{v}{v_0}$ varies by a factor of 50. Therefore, from Equation 13, σ and therefore τ vary by a factor ~5000. All the above variations are consistent with the data. Just the variations in M_0, f_c, and $t_{inter-event}$ can therefore entirely account for our variance in σ and τ.

An example of this variation in the seismic observations can be seen in Fig. S1. Fig. S1 shows two icequake clusters with $\tau \sim 15\ kPa$ and $\tau \sim 1\ MPa$. The difference here in $t_{inter-event}$ is of the order of a factor 10 (see Fig. S1a,b). The difference in corner frequencies is 45 Hz (see Fig. S1c), which is approximately a factor 2, with the difference in τ for the event clusters being approximately a factor 70. This example is therefore consistent with what we suggest above.

We therefore suggest that M_0, f_c, and $t_{inter-event}$ from the seismic observations are the critical parameters that cause the variation in the results that we present in this work.

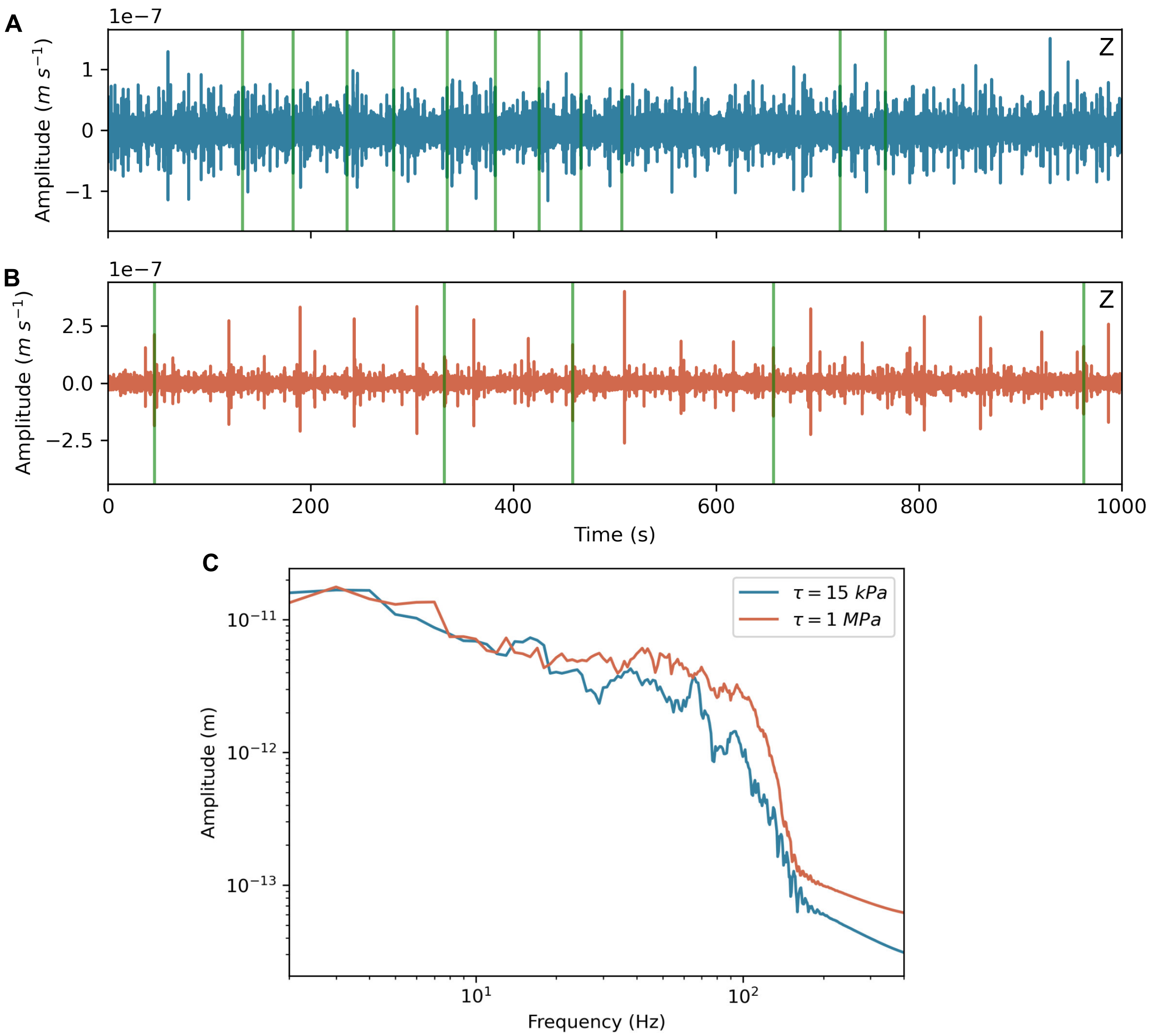

Fig. S1. Examples of waveforms and amplitude spectra for small shear stress vs. large shear stress icequake clusters. (a) Seismic data through time for a cluster with $\tau_{mean} \sim 15\ kPa$. (b) Seismic data through time for a cluster with $\tau_{mean} \sim 1\ MPa$. (c) Spectra for a single event in each time-series in (a) and (b). Data is for receiver R3030, in the centre of the network. Green lines indicate event phase arrival times at the station R3030.

2. Comparison of our results to the parameter space of full rate-and-state model numerical simulations

Our method used to derive basal shear stress, slip-rate and effective normal stress from icequake observations is based on a simplified version of the full rate-and-state friction model. This simplified model assumes that many parameters are temporally-invariant, including the state variable, and so does not involve the calculation of total slip through time, but rather an approximation of it. Although a simplification of the full problem, our approach allows us to directly calculate additional parameters such as the state evolution distance, $\mathcal{L}$, and the effective bed shear modulus, G^*. However, it is also possible to perform numerical simulations that solve the coupled rate-and-state and momentum system of equations, and hence calculate slip, velocity and shear stress explicitly through time. Such numerical simulations require the assumption of more parameters from the outset, but provide a useful way to explore the entire parameter space. Here, we present results from full rate-and-state model numerical simulations, and compare them to icequake observations, in order to ascertain whether our simplified version of the rate-and-state model is valid and consistent with the full model.

The numerical model used to produce the simulations shown here is as follows, based on a model from the literature[19]. All parameter definitions are consistent with their labelling in the rest of this work. The model is based on numerically solving the time-derivative of the momentum equation, Newton's second law, which is given by,

$$\boldsymbol{F} = m \, . \, \boldsymbol{a} \quad (20),$$

where $\boldsymbol{F}$ is the force acting on a block that is allowed to slide over an interface, m is the mass of the block and $\frac{\partial v}{\partial t}$ is the acceleration of the block, with $\boldsymbol{v}$ being the velocity vector. This equation can be rewritten for the 1D case as,

$$F_d - F(v, \bar{\sigma}, \theta) = \eta v \quad (21),$$

where the left hand side equates to the forces acting per unit area on the block. F_d is the driving shear force, which is defined as,

$$F_d = k\,(y - x) \quad (22),$$

where k is the spring constant of the system, y is the displacement of the driving load, and x is the displacement at the slip interface. $F(v, \bar{\sigma}, \theta)$ is the rate-and-state dependent frictional force that resists motion. The original formulation of $F(v, \bar{\sigma}, \theta)$ does not allow for a solution at $v = 0\ m\ s^{-1}$, so we use a regularized formulation[81,82] given by,

$$F(v, \bar{\sigma}, \theta) = \bar{\sigma}\,\mathrm{asinh}^{-1}\left(\frac{v}{2v_0} e^{\frac{\theta}{a}}\right) \quad (23).$$

η in Equation 21 is the radiation damping factor for slip, which is given by[81],

$$\eta = \frac{G^*}{2\,c_S} \quad (24),$$

where c_S is the shear-wave speed. If one of the driving force or velocity F_d or v_d are specified through time, then one can use Equation 21 to calculate v, θ, d and τ through time, using the following system of ODEs. The first describes the displacement, or slip, at the interface and is given by,

$$\frac{\partial x}{\partial t} = v. \quad (25),$$

where v is specified algebraically from Equation 21. The second ODE describes how the loading velocity varies with time and is given by,

$$\frac{dy}{dt} = v_{driving} \quad (26),$$

where $v_{driving}$ is the loading velocity through time. In our case, we set this as constant so it is not solved for. Alternatively, one could set F_d as constant and allow $v_{driving}$ to vary. The third ODE describes the evolution of the state variable through time, and is given by,

$$\frac{d\theta}{dt} = G(v, \theta) \quad (27),$$

where $G(v, \theta)$ can be defined either by the slip law or the aging law. We use the aging law in the form,

$$G(v, \theta) = \frac{b\, v_0}{\mathcal{L}} \left(e^{\frac{\mu_0 - \theta}{b}} - \frac{v}{v_0} \right) \quad (28).$$

Table S2 summarizes the parameters (and their range where appropriate) used in the following simulations and Figure S1 shows the outputs of one simulation of the numerical model as an example of how the system behaves through time.

Parameter	Value (or range)
$\bar{\boldsymbol{\sigma}}$	$10^4\ to\ 10^8\ Pa$
$\boldsymbol{G^*}$	$7 \times 10^7\ to\ 3 \times 10^9\ Pa$
$\boldsymbol{\rho}$	$917\ kg\ m^{-3}$
$\boldsymbol{R}$	$10\ m$
$\boldsymbol{v_{driving}}$	$1.1\ m\ day^{-1}$
$\boldsymbol{v_0}$	$v_{driving}$
$\boldsymbol{a}$	0.005
$\boldsymbol{b}$	0.015
$\boldsymbol{\mathcal{L}}$	$1 \times 10^{-6}\ m$
$\boldsymbol{\mu_0}$	0.4

Table S2. Table of the parameters used in the rate-and-state numerical simulations.

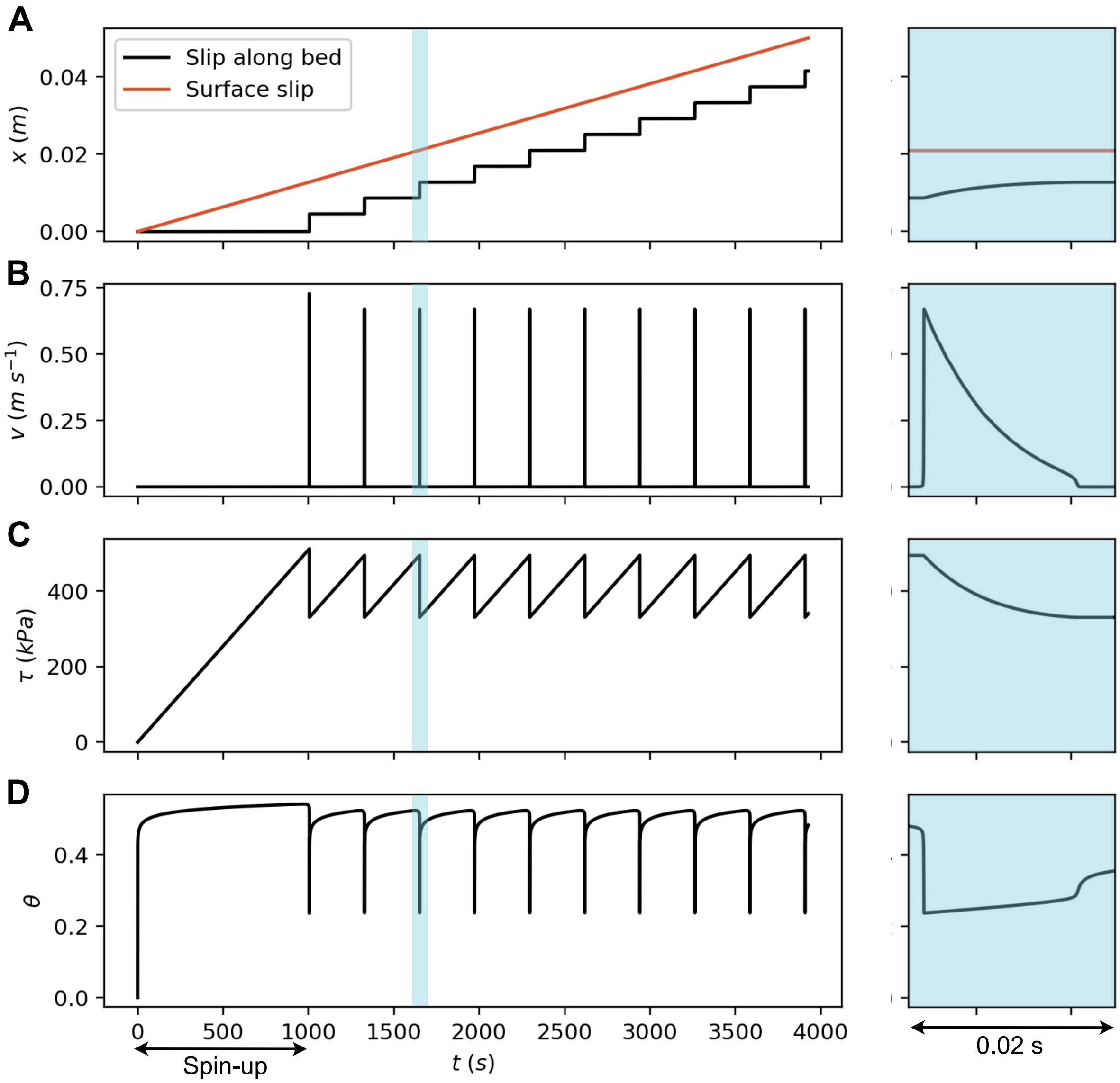

Fig. S2. Example of solution for a numerical rate-and-state model simulation. (a) Driving displacement (red line) and the associated rate-and-state slip (black line) through time. (b) Instantaneous slip velocity through time. (c) Shear stress through time. (d) State variable through time. Blue interval corresponds to inset figures on the right, showing a single slip event in detail. Results are plotted for $\sigma = 1\ MPa$ and $G^* = 0.4\ GPa$.

The results of the full numerical rate-and-state model simulations are summarized in Fig. S3 and Table S3. Fig. S3 shows the simulation predictions of three parameters that can be directly observed from icequake observations without any rate-and-state behavior assumptions: corner-frequency; inter-event time; and stress-drop. Corner-frequency is calculated from $f_c = \frac{v_{FWHM}}{d_{slip}}$ where v_{FWHM} is the half-maximum amplitude of the near-instantaneous velocity change during a single slip cycle, which is used instead of the absolute maximum in an attempt to compensate for near-source effects. The inter-event time is the time between slip cycles and the stress-drop is the near-instantaneous drop in shear-stress during a slip event. Corner-frequency, inter-event time and stress-drop are plotted for 800 simulation runs over a range of shear moduli, G^*, and effective normal stresses, $\bar{\sigma}$. The regions where G^* and $\bar{\sigma}$ are consistent with individual observables are delineated by black-dashed lines, with the blue solid line in each plot in Fig. S3 showing the region where G^* and $\bar{\sigma}$ are consistent with all the icequake observables. The grey region is where $\frac{k}{k_{crit}} > 1$, where the system is conditionally stable and icequakes cannot be generated[32]. The blue dashed line delineates the $f_c < 80\ Hz$ contour, which is the case for the majority of icequakes (see Extended Data Fig. 2).

Additionally, we investigate the effect of varying the state evolution distance, $\mathcal{L}$, on the numerical simulations, to see if varying $\mathcal{L}$ affects the predicted shear and normal stresses. The results are shown in Fig. S4. White regions indicate areas where the simulations are conditionally stable and therefore aseismic. Varying $\mathcal{L}$ has no effect on which simulations agree with the icequake observations, since it doesn't affect predicted inter-event times, which provide critical constraint on the comparision between observations and simulations. However, as $\mathcal{L}$ increases, the bed has to be weaker in order to be unstable and sustain seismic failure. Of particular note are the plots in Fig. S4g,h, which are for $\mathcal{L} = 7 \times 10^{-5}\ m$, the value found from the analysis in the main text. Note that the conditionally stable region-unstable transition corresponds to the lower limit of normal stress for which icequakes can be generated. This provides further evidence to justify our assumption that the icequakes that we observe likely occur at shear stresses only just greater than the conditionally-stable to unstable transition.

The overall conclusion from the numerical simulations is that all the icequake observables are consistent with a full rate-and-state model (see Table S3). Although the ranges span orders of magnitude, similar to our findings in the main text, the simulations do provide additional constraint on the lower and upper bounds of both $\bar{\sigma}$ and τ. Notably, the upper bound of $\bar{\sigma}$ is half the upper bound suggested from the observations presented in the main text, somewhat reducing the potential controversy of anomalously high $\bar{\sigma}$. However, $\bar{\sigma}$ is still significantly higher than any previously observed normal stresses from borehole measurements, which we argue is acceptable in the main text. We cannot assess whether slip-rates are reasonable as we fixed the driving velocity as the reference velocity. However, we deem this acceptable as the majority of our slip-rate observations agree with this value, within uncertainty.

Overall, the full numerical rate-and-state simulations conclusively agree with the observations we derive from our simplified rate-and-state model calculations in the main text. We therefore argue that both the simplified method and the numerical simulation approach are self-consistent and therefore equally valid. One could therefore justify either philosophy when approaching the problem set out in this study. We favor the simplified method as we can rigorously propagate uncertainties through the algebraic expressions.

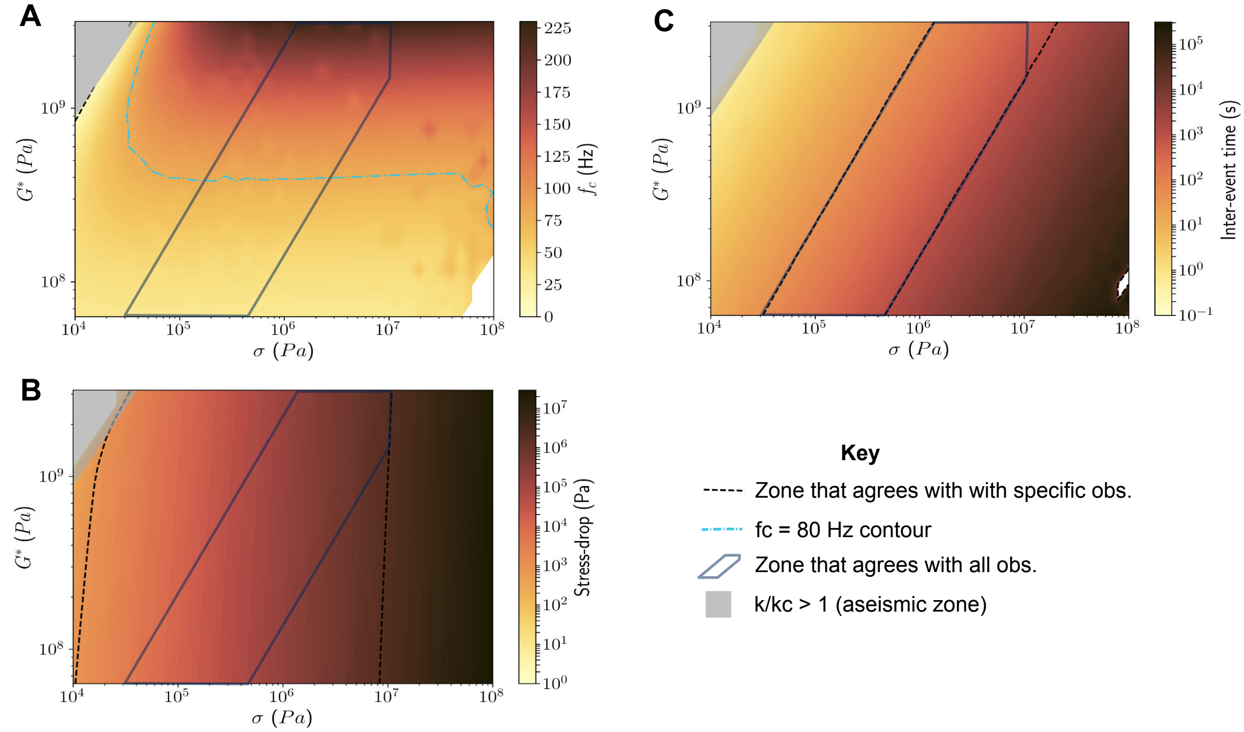

Fig. S3. Predictions of key icequake observables from rate-and-state model numerical simulations. (a) Plot of predicted icequake corner frequency with varying effective bed shear modulus, G^*, vs. effective normal stress, σ. Corner frequency is calculated using the predicted slip and the full width half maximum of the maximum predicted velocity during that slip episode. Blue dashed line delineates the $f_c = 80\ Hz$ contour, with the majority of observed icequake $f_c < 80\ Hz$ (see Extended Data Fig. 2). (b) Same as (a) but for stress-drop. (c) Same as (a) but for inter-event time. Black dashed lines delineate regions within which real icequake observations fall. Blue solid line indicates the region of G^*- σ model space that fits all the combined icequake observables.

	$v_0\ (m\ day^{-1})$	$G^*\ (GPa)$	$\bar{\sigma}\ (kPa)$	$\tau\ (kPa)$
Lower bound from numerical model	1.1	0.07	30	16
$f_c = 80\ Hz$ contour	1.1	0.4	3000	2200
Upper bound from numerical model	1.1	3.0	9000	5600

Table S3. Lower and upper bounds of key basal parameters. Parameters are constrained based on the comparison of numerical rate-and-state model simulation predictions for key icequake observables with the corresponding actual observed icequake parameters (see Figure S1). Note that v_0 is fixed at the driving velocity, specified to be equal to the surface velocity in the simulations.

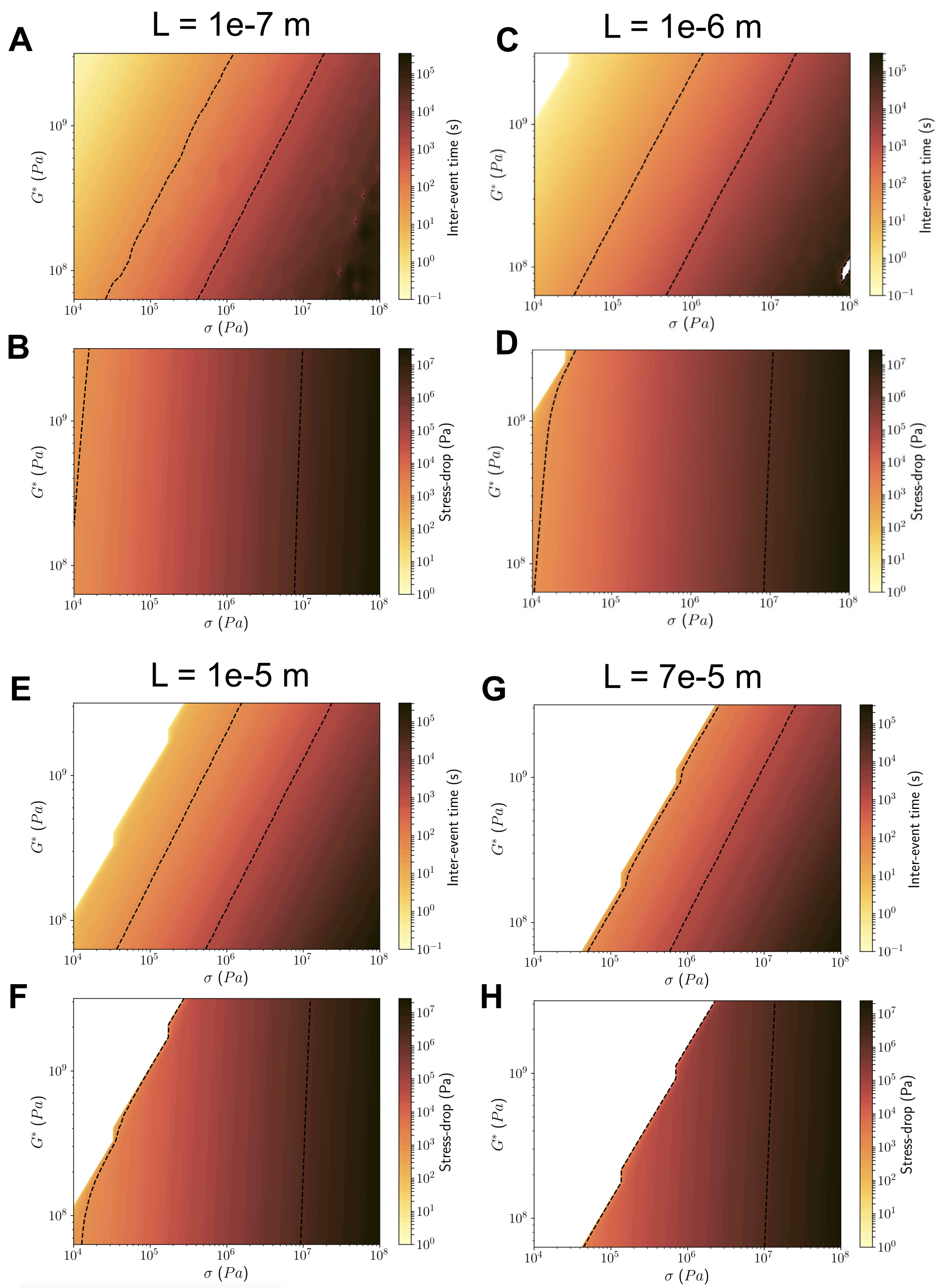

Fig. S4. Rate-and-state numerical simulations for varying state evolution distance, $\mathcal{L}$. Inter-event time and stress-drop for various values of $\mathcal{L}$. (a),(b) Inter-event time and stress-drop, respectively, for $\mathcal{L} = 1 \times 10^{-7}\ m$. (c), (d) Same as (a),(b) but for $\mathcal{L} = 1 \times 10^{-6}\ m$. (e), (f) Same as (a),(b) but for $\mathcal{L} = 1 \times 10^{-5}\ m$. (g), (h) Same as (a),(b) but for $\mathcal{L} = 7 \times 10^{-5}\ m$ (same value as main study).

3. A note on the choice of $(\boldsymbol{a}-\boldsymbol{b})$ in the rate-and-state friction model and associated implications

In this work, we have had to make assumptions and fix certain values in the rate-and-state friction formulation to make the problem mathematically tractable. One of the most significant assumptions made is arguably the choice to fix $(\boldsymbol{a}-\boldsymbol{b})$ rather than $\bar{\sigma}$ in Equation 9. One of these two values has to be fixed, as they trade off in the transient frictional component of the equation. One could argue to fix either. $(a-b)$ could be fixed at an assumed appropriate value from the literature, but this could lead to errors in the results if the value is actually not representative of the system or if the system cannot be described adequately by a temporally- and spatially- static value. Alternatively, one could fix $\bar{\sigma}$ to a single value, such as that measured independently, in the case of a glacier perhaps from a borehole bed pressure measurement. However, in fixing $\bar{\sigma}$ one implicitly assumes that the normal-stresses are homogeneous across the bed in both space and time. In the main text, we assume a constant $(a-b)$, based on the assumption that $\bar{\sigma}$ is more likely to vary by a greater extent than $(a-b)$. However, here we test whether that assumption is valid and what effect varying $(a-b)$ rather than $\bar{\sigma}$ has on the main findings.

Figure S1 summarizes how key results of this study vary depending upon whether $(a-b)$ or $\bar{\sigma}$ is the free parameter. Figure S1a shows the distribution of $(a-b)$ for all the icequakes in the study if $\bar{\sigma}=0.188\ MPa$, from borehole measurements[83]. If this normal stress is approximately accurate through space and time, then the results suggest that $(a-b)$ can vary by more than one order of magnitude, with the mode lying at $(a-b)\approx -0.001$. This value lies at the lower bound of typical values for rock-on-rock friction[81,84] as well as a value found by experiment for debris-laiden ice[85]. Notably it is one order of magnitude lower than the value assumed in the analysis presented in the main text of this study, although both values just lie within the suggested range of possible values from literature.

The results of Figure S1a prompt the question of how might the normal stresses and slip rates vary if we fixed $(a-b)=0.001$ instead of $(a-b)=0.01$. A summary of the results are shown in Figure S1b and S1c. Figure S1b clearly demonstrates the linear relationship between $(a-b)$ and $\bar{\sigma}$, where if $(a-b)$ is decreased then $\bar{\sigma}$ has to increase. The clear bimodal distribution obviously remains unchanged. However, the upper, smaller distribution for $(a-b)=0.001$ lies an order of magnitude above the maximum possible ice overburden pressure of 18.9 MPa. While this upper limit could potentially be exceeded based on the Regime I slip hypothesized in Figure 5 of the main text, we prefer the interpretation that $(a-b)=0.001$ is too low for at least the majority of the bed. We prefer this interpretation based on the clear upper limit in $\bar{\sigma}$ exhibited in the $(a-b)=0.01$ distribution at $\sim 20\ MPa$.

While the results of Figure S1b suggest that our original $(a-b)$ estimate is appropriate if $(a-b)$ is fixed, the question as to whether it is valid to fix $(a-b)$ remains open. The data presented in Figure S1c present perhaps the most compelling evidence for fixing $(a-b)$ rather than $\bar{\sigma}$. The difference in shape of the distributions in slip-rate for the fixed $\bar{\sigma}$ compared to the fixed $(a-b)$ cases is considerable. The fixed $\bar{\sigma}$ results have a mode of zero slip-rate, and a mean $<< 1\ m\ day^{-1}$, whereas for fixed $(a-b)$ the peak and mean slip-rates are $\sim 0.7\ m\ day^{-1}$ and $\sim 1\ m\ day^{-1}$, respectively. These latter values are in much closer agreement with observed surface slip-rates of $\sim 1.1\ m\ day^{-1}$. Furthermore, the fixed $(a-b)$ distribution is what should be expected physically, with a significant proportion of the slip accommodated seismically by certain patches of the bed over up to several days in duration. We argue that the concept of the seismically active sticky-spots accommodating negligible slip over durations of days is unlikely. We therefore favour fixing $(a-b)$ rather than $\bar{\sigma}$ in this work.

In an ideal scenario, one would vary both $(a-b)$ and $\bar{\sigma}$ simultaneously. Although we cannot present a method for undertaking this in a mathematically tractable way using our approach, it may well be possible, especially if applying a fully time-varying rate-and-state slip model. In order to somewhat accommodate the possibility of $(a-b)$ varying considerably, we incorporate an estimate of the uncertainty in $(a-b)$ into our results. In the absence of better constraint, we set the uncertainty, $\alpha_{a-b} = 0.005$, corresponding to a 50% error in the fixed value of $(a-b)$ used in this work. However, our findings would benefit from further experimental constraint of the possible variation $(a-b)$ parameter for similar bed conditions to that of Rutford Ice Stream, which are not readily available at present.

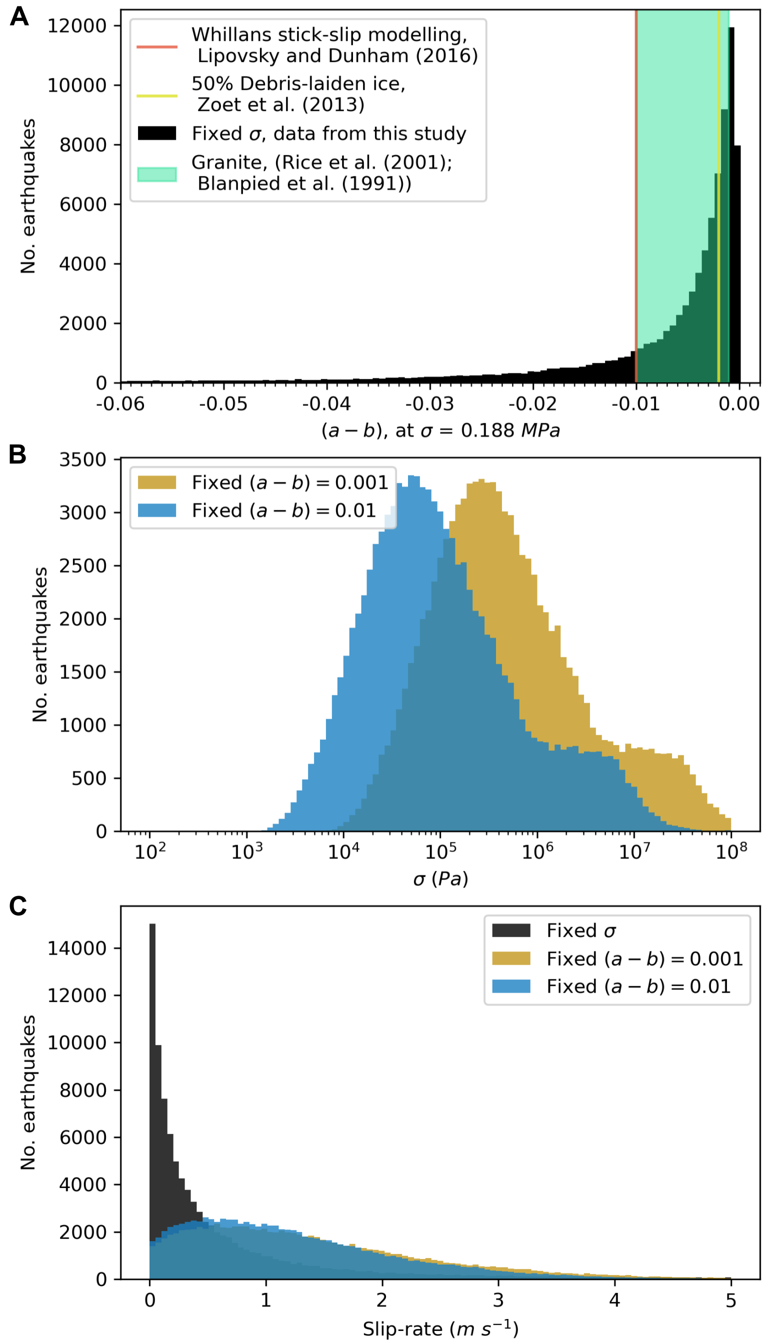

Fig. S5. Effect of varying $(\boldsymbol{a}-\boldsymbol{b})$ vs. varying $\boldsymbol{\sigma}$ on the results of this study. (a) Histogram of $(\boldsymbol{a}-\boldsymbol{b})$ for every icequake, if $\boldsymbol{\sigma}$ is fixed rather than $(\boldsymbol{a}-\boldsymbol{b})$. $\boldsymbol{\sigma}$ is fixed at $\mathbf{0.188}\ \boldsymbol{MPa}$ the average normal stress observed at the bed from borehole measurements[83]. Red line shows $(\boldsymbol{a}-\boldsymbol{b})$ value used in this work, based on literature[19], yellow line shows a value found by experiment for debris-laiden ice[85] and the green region shows the range of values expected for rock-on-rock friction[81,84]. (b) Histogram showing the effect of fixing $(\boldsymbol{a}-\boldsymbol{b})$ on $\boldsymbol{\sigma}$ for the different extremes of the $(\boldsymbol{a}-\boldsymbol{b})$ ranges shown in (a). Blue data are for the value used in the main text. (c) Histogram showing the effect of varying $(\boldsymbol{a}-\boldsymbol{b})$ compared to varying $\boldsymbol{\sigma}$ on slip-rates.

4. A note on the stability of the rate- and state- friction model

A glacier sliding law must obey two fundamental principles: the sliding law cannot be unstable, i.e. it cannot lead to runaway acceleration of ice into the ocean on unphysical timescales; and it has to apply to bed-types observed at a glacier, i.e. deformable and/or hard beds. The applicability to relevant spatial scales is also important.

The rate- and state- model we use to explain stick-slip motion in this study can also describe steady-state motion at a frictional interface. Theoretically, the parameters in the governing equations (Equation 5, Equation 9) can describe both hard and deforming beds. However, the rate dependence of the model could lead to an unstable model that would be unphysical. There are two components of the rate- and state- friction model that dictate whether the model is stable, conditionally stable, or unstable [32]. The first component is the $(a - b)$ term. If $(a - b) > 0$ then the model is described as velocity-strengthening. a and b are dependent on material and fault parameters. However, in our case, $(a - b) < 0$ [19], a necessary condition for velocity-weakening behavior, which is required to facilitate the stick-slip behavior required to generate seismicity [32]. The second model component is more subtle and is the critical effective normal stress, $\overline{\sigma_c}$, the minimum stress required to move from a stable regime to an unstable regime [32], even if the material is inherently velocity-weakening, as hypothesized in this study. Therefore, if the effective normal stress can vary above and below $\overline{\sigma_c}$, then one can generate icequakes in certain unstable patches at certain times while remaining stable elsewhere.

To demonstrate the controls on a rate- and state- friction model's stability, we look at the parameters governing the value that $\overline{\sigma_c}$ takes (see Equation 15). All the parameters are dependent on the material properties and $\bar{\sigma}$ except the fault radius, R. So, assuming that the material composition is approximately homogeneous spatially and temporally, then the relationship between $\bar{\sigma}$ and R demonstrates how a glacier can be stable. Fig. S6 shows this relationship for three values of R, representing the approximate average, lower and upper bounds observed in this study. The region below the red dashed line is stable, and the region above this line is unstable, where stick-slip motion occurs. For the largest observed fault patches ($R = 30\ m$), slip is unstable for almost all conceivable effective normal stresses. However, for the smaller fault patches ($R = 5, 10\ m$) the effective normal stresses required for the friction law to become unstable are higher than the likely effective normal stresses throughout much of the bed at RIS. This simple theoretical test therefore demonstrates that a rate- and state- friction law can meet the required stability criteria if the majority of the bed has low effective normal stresses, and those with higher effective normal stresses are much smaller compared to the total bed area.

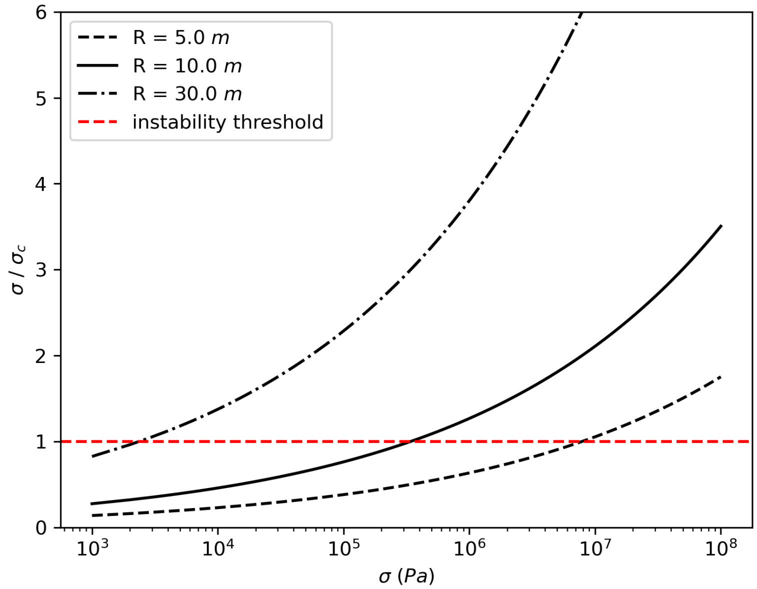

Fig. S6. Effect of fault radius on effective normal stress required to initiate stick-slip behavior. Plot of predicted effective normal stress $\overline{\boldsymbol{\sigma}}$ to critical normal stress required for failure $\overline{\boldsymbol{\sigma_c}}$ vs. effective normal stress $\overline{\boldsymbol{\sigma}}$ for various fault radii. The red dashed line indicates the instability threshold, above which stick-slip behavior theoretically occurs.